The role of synovial fluid constituents in the lubrication of collagen-glycosaminoglycan scaffolds for cartilage repair

AUTHOR(S)

Austyn R Matheson, Eamon Sheehy, Gregory D Jay, W Michael Scott, Fergal O'Brien, Tannin A Schmidt

The Role of Synovial Fluid Constituents in the Lubrication of Collagen-Glycosaminoglycan Scaffolds for Cartilage Repair

Authors:

Austyn R. Matheson, PhD[1]; Eamon J. Sheehy, PhD[2,3,4]; Gregory D. Jay, MD, PhD[5];

W. Michael Scott, MVSc, DVM[1,6]; Fergal J. O'Brien, PhD[2,3,4]; Tannin A. Schmidt, PhD[7]

[1]Biomedical Engineering Graduate Program, University of Calgary, Calgary, AB, Canada.

[2]Tissue Engineering Research Group (TERG), Department of Anatomy and Regenerative Medicine, Royal College of Surgeons in Ireland, Dublin, Ireland

[3]Trinity Centre for Biomedical Engineering, Trinity Biomedical Sciences Institute, Trinity College Dublin, Dublin, Ireland

[4]Advanced Materials and Bioengineering Research Centre (AMBER), Royal College of Surgeons in Ireland and Trinity College Dublin, Dublin, Ireland

[5]Department of Emergency Medicine, Warren Alpert Medical School & School of Engineering, Brown University, Providence, RI, USA

[6]Faculty of Veterinary Medicine, University of Calgary, Calgary, AB, Canada.

[7]Biomedical Engineering Department, University of Connecticut Health Center, Farmington, CT, USA.

* Please address correspondence to Dr. Tannin A. Schmidt, 263 Farmington Avenue, MC 1721, University of Connecticut Health Center Farmington, CT, US, 06030 (tschmidt@uchc.edu)

Abstract:

Extracellular matrix (ECM)-derived scaffolds have shown promise as tissue-engineered grafts for promoting cartilage repair. However, there has been a lack of focus on fine-tuning the frictional properties of scaffolds for cartilage tissue engineering as well as understanding their interactions with synovial fluid constituents. Proteoglycan-4 (PRG4) and hyaluronan (HA) are macromolecules within synovial fluid that play key roles as boundary mode lubricants during cartilage surface interactions. The overall objective of this study was to characterize the role PRG4 and HA play in the lubricating function of collagen-glycosaminoglycan (GAG) scaffolds for cartilage repair. As a first step towards this goal, we aimed to develop a suitable *in vitro* friction test to establish the boundary mode lubrication parameters for collagen-GAG scaffolds articulated against glass in a phosphate buffered saline (PBS) bath. Subsequently, we sought to leverage this system to determine the effect of physiological synovial fluid lubricants, PRG4 and HA, on the frictional properties of collagen-GAG scaffolds, with scaffolds hydrated in PBS and bovine synovial fluid (bSF) serving as negative and positive controls, respectively. At all compressive strains examined (ε = 0.1 - 0.5), fluid depressurization within hydrated collagen-GAG scaffolds was >99% complete at ½ minute. The coefficient of friction was stable at all compressive strains (ranging from a low 0.103 ± 0.010 at ε=0.3 up to 0.121 ± 0.015 at ε=0.4) and indicative of boundary-mode conditions. Immunohistochemistry demonstrated that PRG4 from recombinant human (rh) and bovine sources adsorbed to collagen-GAG scaffolds and the coefficient of friction for scaffolds immersed in rhPRG4 (0.067 ± 0.027) and normal bSF (0.056 ± 0.020) solution decreased compared to PBS (0.118 ± 0.21, both $p<0.05$, at ε=0.2). The ability of the adsorbed rhPRG4 to reduce friction on the scaffolds indicates that its incorporation within collagen-GAG biomaterials may enhance their lubricating ability as potential tissue-engineered cartilage replacements. To conclude, this study reports the

development of an *in vitro* friction test capable of characterizing the coefficient of friction of ECM-derived scaffolds tested in a range of synovial fluid lubricants and demonstrates frictional properties as a potential design parameter for implants and materials for soft tissue replacement.

Highlights:

- A scaffold-on-glass friction test for determining the coefficient of friction of ECM-derived biomaterials immersed in different synovial fluid lubricants was developed.
- Boundary mode lubrication conditions were established by demonstrating fluid depressurization of the scaffolds after compressive loading, and an invariant scaffold coefficient of friction over a range of compression strains.
- rhPRG4 adsorbed onto collagen-GAG scaffolds in a functionally determinant manner reducing its coefficient of friction.
- The incorporation of rhPRG4 within scaffolds may enhance their lubricating ability as tissue-engineered cartilage replacements.

Key Words:
Tissue-Engineered-Cartilage; Collagen-Scaffold; Lubrication; PRG4; Hyaluronan; Synovial Fluid;

1. **Introduction**

Tissue-engineered cartilage aims to regenerate or replace damaged tissues through a combination of cells, signaling molecules, and scaffolds[1]. Three-dimensional scaffolds, typically fabricated using synthetic or natural polymers, are designed to possess both the biological and biomechanical specifications of native components. Biologically, scaffolds should promote cellular integration, chondrogenic differentiation, and synthesis of new matrix before finally degrading into non-toxic bi-products[2]. Biomechanically, scaffolds must remain structurally intact within the complex joint loading environment until full tissue-integration and repair is complete[3,4]. The predominant function of cartilage is to support the nearly frictionless articulation during locomotion. However, little focus has been given to the frictional properties of tissue-engineered implants[5]. Indeed, the recommended mechanical characterization of cartilage implants by the FDA (ASTM F2451-05-2010) describes uniaxial-steady compressive tests derived from reports that are over thirty years old. This has led to a limited understanding of the frictional properties of synthetic or natural polymers used for soft tissue replacement[6,7,8]. The explanation for the lack of material tests in a multi-axial and dynamic configuration is manifold. Challenges include the expense of mechanical test equipment and software, the time for developing and validating a custom setup and protocol, the variability of biological samples, challenges in sample preparation, and finally, relatively 'soft' biological materials that require sensitive equipment resolution to characterize differences between test groups. Regardless of these collective challenges, advances in test setups are necessary to establish physiological methods to validate materials and establish industry standards for the frictional characteristics of tissue-engineered cartilage.

97 The lubrication of articular tissues occurs through theoretical (and experimentally tested)
98 mechanisms[9,10,11,12] over several apparent modes[13,14,15]. Cartilage tissue is biphasic, providing an
99 initially low friction coefficient, owing to hydrostatic load support upon the onset of tissue loading
100 followed by increasing friction coefficient to an equilibrium value as fluid load support
101 depressurizes[16]. If cartilage at contact interfaces can maintain fluid pressurization, as with a
102 migrating contact area, the friction coefficient remains very low[17,18]. However, if fluid load support
103 depressurizes as with a stationary contact area, the boundary mode lubrication dominates as
104 surfaces articulate in direct contact[11]. The coefficient of friction in boundary mode lubrication is
105 invariant over a range of compressive loads, entraining speeds, and lubricant viscosities[19]. This
106 mode is consistent with the highest friction and wear rates observed[20], and synovial fluid
107 biomolecules at the cartilage surface are critical to maintaining low friction. In particular, synovial
108 fluid constituent's proteoglycan-4 (PRG4) and hyaluronan (HA) are boundary lubricants which
109 reduce articular surface interactions (friction and surface shear strain)[19,21]. Cartilage lubrication
110 mode plays a significant role in the friction coefficient and, therefore, tissue shear stress at the
111 articular surface, properties known to induce anabolic and catabolic responses from chondrocytes
112 within cartilage tissue[22,23,24]. Therefore, clarifying *in vitro* scaffold lubrication by physiological
113 lubricants may aid scaffold design considerations.

114

115 Collagen is an attractive natural polymer for use as a scaffold in tissue engineering applications as it
116 is the main component of the extracellular matrix (ECM) and contains binding sites for cells (ligands)
117 on its surface[25,26]. Furthermore, the addition of ECM molecules such as glycosaminoglycans (GAGs)
118 to produce collagen-based composite scaffolds support the chondrogenesis of mesenchymal stem
119 cells (MSCs) *in vitro*[27,28,29,30]. When used as the top chondral layer of a tri-layered scaffold, cell-free

collagen-GAG scaffolds promote cartilage regeneration in both small (rabbit) and large (goat and horse) pre-clinical models[31,32,33]. However, the quality of repaired tissue observed in these studies could potentially be further improved by enhancing the frictional qualities at the surface of implants, thereby protecting the tissue from the repeated forces (shear stress) of normal joint articulation. If not primed to support lubrication, the high friction, and shear stress at the surface of cartilage replacements and the regenerated matrix could lead to adverse cell metabolism and apoptosis[22,23,24], the undue wear of cartilage implants or regenerated tissue, risk of fibrocartilage formation, or possibly damage to opposing cartilage surfaces[34]. The extent to which these events could arise from elevated friction and shear stress during joint articulation is unclear as there is no information on the frictional properties of collagen-GAG scaffold interfaces.

The structure of freeze-dried collagen-GAG scaffolds can be modeled as porous open-cell foams[35] with tested deformation mechanisms and stress-strain behavior within uniaxial compression[36] and tension configurations[35]. In compression[36], three distinct regimes divide the stress-strain curves for low-density, open-cell foams: a linear elastic regime (controlled by strut bending), a collapse plateau regime (struts buckling and pore collapse) and a densification regime (complete pore collapse throughout the material). Transitions between linear elastic to collapse-plateau regions occur at roughly $\varepsilon = 0.1$ strain for collagen scaffolds, with densification occurring at high strains ($\varepsilon = 0.8$). In tension, collagen matrices have similar responses in the linear-elastic regime. However, with increasing tension, struts become increasingly oriented in the direction of the applied tension, and the stiffness of the material increases until tensile failure with strain-rate dependent response[37]. Compressive strains that result in pore collapse and material densification alter hydraulic

permeability and may have significant effects on the dominating lubrication-mode for collagen-GAG scaffold implants.

The overall objective of this study was to characterize the role of synovial fluid and its constituent's (PRG4 and HA) on the coefficient of friction of collagen-GAG scaffolds for cartilage repair. As a first step towards this goal, we sought to develop a suitable *in vitro* friction test to establish boundary mode lubrication parameters by evaluating the frictional properties of collagen-GAG scaffolds articulated against glass over a range of compression strains. Subsequently, this test was leveraged to characterize the lubricating-ability of collagen-GAG scaffolds immersed in different synovial fluid lubricant solutions, as an elucidation of the role such macromolecules play in lubrication may allow for the future development of biomaterials with optimized frictional properties .

2. **Methods and Materials**

2.1 Sample Preparation

2.1.1 Collagen-GAG Slurry

Collagen-GAG slurry was prepared as described previously[36]. The day before blending, 0.5 M acetic acid was mixed by diluting 22.9 mL glacial acetic acid to 800 mL distilled deionized water (d.d.H_2O) and adjusted to a pH 3.2. First, 1.8 mg (dry weight) of micro-fibrillar bovine tendon collagen-I (Collagen Matrix, Franklin lakes, NJ, USA) was chopped and placed into 300 mL 0.5 M acetic acid at 4°C overnight. Separately, 0.16 mg sodium salt hyaluronic acid (0.74-1 MDa, Sigma-Aldrich, Arklow, Co. Wicklow, Ireland) was added to 60 mL 0.5M acetic acid and incorporated by placing conical tubes onto tube rollers at 4°C overnight. The following day, the collagen-only solution was thoroughly mixed with an overhead blender (Ultra Turrax T18 Overhead blender, IKA Works Inc., Wilmington, NC) at 15000 RPM for 90 minutes. The hyaluronic acid solution was added to the collagen-solution with ongoing overhead blending (dropwise in 5-10 mL increments every 10-20 minutes to prevent coagulation). Throughout mixing, the slurry beaker was kept immersed in an ice bath to prevent protein denaturation from the heat released by the blender.

2.1.2 Collagen-GAG Scaffold Fabrication

The collagen-GAG slurry was de-gassed under vacuum to remove bubbles introduced during mixing and loaded onto stainless-steel molds. The stainless-steel molds were designed to produce cylindrical scaffolds (10 mm outer diameter x 8 mm height, 800 µL slurry per scaffold). Loaded molds were then placed onto machine shelves (Advantage EL, Vir-Tis Co., Gardiner NY). The lyophilization schedule initiated at 20°C to normalize conditions, then the shelf was cooled at

0.9°C/min to a final freeze temperature of -40°C[38] . The final freeze temperature was held for 1 hour (ice crystals form, slowly trapping collagen outside) , followed by sublimation and heating in primary and secondary phases to release both free and bound water from the matrix. The entire lyophilization cycle was completed within 25 hours. Collagen-GAG scaffolds were produced with a high level of porosity and a homogenously interconnected pore architecture[39,40] (pore sizes and surrounding collagen struts mirror the final ice crystal structure).

2.2 Synovial Fluid Lubricant Solutions

For mechanical tests, the lubricant solutions included: 1X phosphate-buffered saline (PBS) (negative control), individual synovial fluid constituent solutions (recombinant human (rh) PRG4 and HA) at physiological concentrations[21], and normal bovine synovial fluid (bSF) (positive control) (Animal Technologies Inc., Tyler, TX, USA). Purified full-length rhPRG4, obtained from Lμbris BioPharma LLC., (Framingham, MA, USA)[41], was diluted to 450 μg/mL in PBS. HA solution was prepared by dissolving and gently incorporating (tube rotation, 24 hours) 1.5 MDa HA (Lifecore Biomedical, Chaska, MN, USA) at a physiological concentration of 3.33 mg/mL in PBS.

2.3 Scaffold-on-Glass Friction Test

2.3.1 Mechanical Tester Specifications

All mechanical tests were completed on a Mach-1 mechanical tester v500csst (MA009, Biomomentum, Laval, QC, Canada), with a multi-axial load cell and 17N amplification module (MA232, Biomomentum), and sample base chamber (50.8 mm) (MA626, Biomomentum). The Mach-1 is a configurable machine, with sensitive resolution ($F_z \pm 0.85$ mN, $F_{x,y} \pm 0.60$ mN, $T_{x,y,z} \pm 6.0$

206 μN•mm), and the capability to execute repeatable sequences. All tests were completed at room
207 temperature. In preparation for friction testing, adhesive sandpaper (grit-100) was superglued to
208 the sample base chamber the day prior. To prepare the glass-counterface, microscope cover glasses
209 (Fisherbrand 12-545-102 25CIR-1) were superglued to cap-screws (1/4" 28 x 1-¼", Everbilt Grade 5 –
210 Fine screw - Zinc). The equipment and sample setup are depicted below (**Fig. 1)**. Prior to loading
211 components, the multi-axial load cell was calibrated according to manufacturer's instructions.
212 Following calibration, the sample base was secured to the stage and the mounted glass cover slip
213 secured to the load cell. A find contact function was used to set the vertical stage position with
214 reference to the sample base chamber and glass counter face. The load cell was zeroed and moved
215 at 0.05mm/s until an axial force of 100 mN was detected (to ensure full contact between glass
216 cover slip and the base chamber) and the position was set to 0 mm as a reference.

217 For all mechanical tests, collagen-GAG scaffolds were pre-hydrated in PBS and then placed in a test
218 lubricant bath (PBS, rhPRG4 solution, HA solution, or bSF) for 1-3 hours prior to testing. During,
219 hydration, scaffolds lose some aspects of the original "dry" shape and decrease in size, and so, prior
220 to loading samples onto the test set-up, the top point on the hydrated scaffold (resting on a flat
221 surface) was measured with calipers. To measure the sample height (with complete glass- contact),
222 a hydrated scaffold was centered on the sample base chamber, and the glass counter face brought
223 close to contact (~ 0.2 mm). The sample chamber was filled with test lubricant to replenish the
224 sample for 1 minute. The sample height was determined by a find contact function. The load cell
225 was zeroed (with the indenter fully immersed in the test solution, and taring both force ($F_{x,y,z}$) and
226 torque ($T_{x,y,z}$) and moved at 0.02mm/s until an axial force of 2 mN was detected, and therefore
227 sample contact was made. Sample height was recorded to calculate compressive strain (ε) and
228 velocity (v_{down}) for subsequent mechanical testing. According to these measurements, samples were

compressed from the top height measured by calipers by approximately 5.75±2.37% (bathed in rhPRG4) up to 8.08±1.61% (bathed in PBS) (% ± SEM) using the find contact function. The measured scaffold heights (by find contact) were not significantly different (1-way ANOVA, $p>0.05$). Sample heights were 5.3±0.32 mm in PBS, 6.14±0.18 mm in HA, 5.13±1.17 mm in rhPRG4, and 5.24±0.59 mm in bSF.

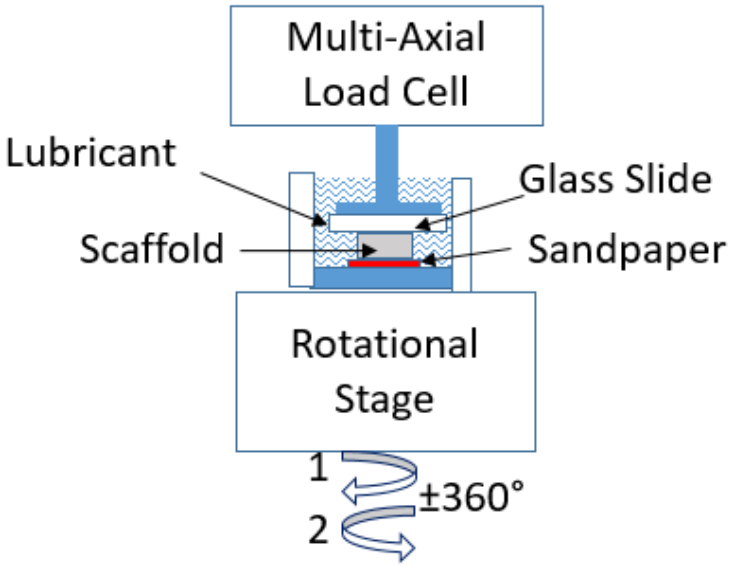

Figure 1: The equipment and sample setup for scaffold-glass friction test.

2.3.2 Test Parameters

The test configuration for collagen-GAG scaffolds was a stationary contact rotational test, against a glass counterface, adapted from tests as described previously[19,42,43]. The stationary contact rotational set-up minimizes hydrodynamic effects generated by a leading edge and changing contact areas, shown in other set-ups (e.g., pin on disc) and undesirable for boundary mode conditions. Indeed, a rotating annulus on disc configuration has been employed previously to study

cartilage-cartilage[19,42] and cartilage-glass boundary lubrication[43]. During testing, scaffolds were kept in place by sandpaper glued to the bottom of sample-base holders and articulated against the glass counterface. Samples were compressed at a constant velocity downwards v_{down} = 2% of height per second. Compression (ε) refers to the normal strain applied to samples, presented here in absolute terms. Stress relaxation duration refers to the hold time for fluid depressurization post-compression. Subsequently, samples were rotated ±360° at a slow angular velocity of ω = 7°/second to maintain boundary mode lubricating conditions. The effective sliding velocity ($v_{eff} = \omega R$), increases from approximately zero at the center (R = 0mm) up to 0.6 mm/s at the outer radius (R = 5mm), conditions shown to be suitable for boundary lubrication at cartilage-cartilage interfaces[42] and on the same order as other friction test setups[44]. The following sequence was completed on scaffolds (n=5) to determine the effect of compression and test parameters for subsequent experimental tests (**Fig. 2**). All data were collected at a frequency of 100 Hz.

i. Compressive strain: ε = 0.1, 0.2, 0.3, 0.4, and 0.5.
ii. Stress relaxation duration: ½ minute.
iii. Angular velocity: ω = 7 °/second or 1.16 rpm.
iv. Rotational displacement: ±360°.
v. Release sample and wait for 5 minutes before completing next compression step-ramp.

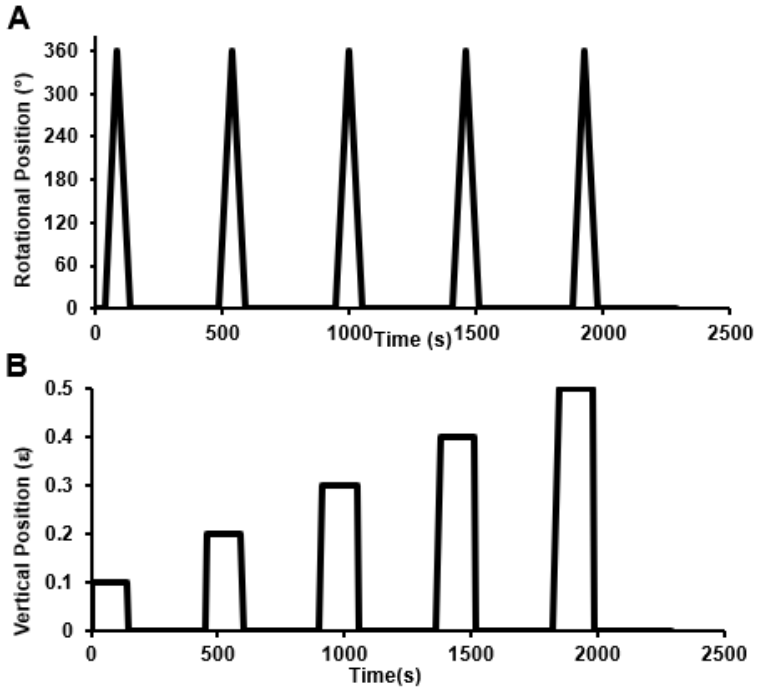

Figure 2: The rotational (**A**) and vertical (**B**) positions versus test time, total time 33 minutes.

2.4 Data Analysis

The kinetic coefficient of friction ($\mu_{kinetic,\,Neq}$) was calculated as follows:

$$\mu_{kinetic,Neq} = {\tau_Z|}\Big/{r \times F_{N,equilibrium}}$$

The absolute torque ($|\tau_Z|$) was calculated from torque measured in both the positive rotation (from 100° to 260°) and the negative rotation (260° to 100°) as $|\tau_z| = (\tau_{z,positive} - \tau_{z,negative})/2$, thereby accounting for offset torque. The scaffold radius (r) was 5 mm. The normal equilibrium load ($F_{N,\,equilibrium}$) was calculated from the linear portion of the curve after stress relaxation.

The compressive stiffness of scaffolds was determined from data obtained during the ramp loading. Collagen-GAG scaffolds were compressed to ε=0.2 strain in unconfined wet compression at v_{down}=

2% height per second (n=5). The compressive stiffness of samples was calculated by simple linear regression of stress-strain curves (ε=0.02-0.09) from data obtained during the ramp loading. The normalized stress-relaxation data was fit to the stretch exponential model[45,46] (**Equation 1**), that accounts for the polymeric mechanism of relaxation. The stretch exponential model has been used to describe the viscoelastic relaxation of a wide range materials including cartilage[47,48] and cells encapsulated in a agarose gel micro-environment[49] . The model is a time-dependent viscoelastic model suitable for unconfined compression behaviour analysis, the conditions under which the data was acquired.

$$\sigma = \left(\sigma_{peak} - \sigma_{eq}\right) e^{-\left(\frac{t}{\mathrm{T}}\right)^{\beta}} + \sigma_{eq} \qquad \textbf{(1)}$$

The value for σ_{peak} was determined experimentally, lower case "t" represents time. The coefficients, T and β, and σ_{eq} were quantified by fitting experimental data to the model (**Equation 1**) using nonlinear optimization to minimize the sum square of weighted residuals (R function: nlsLM, package: minpack.lm). The stress relaxation time constant (T) is associated with physical characteristics of the test set up and viscoelasticity of materials (for example, temperature, polymer length, and concentration). The stretching parameter (β) is related to the type of polymer motion, e.g. reptation, and is inversely proportional to changes in polymer length. All analyses of raw .txt files were completed using a custom analysis program on RStudio (version 1.2.5033).

2.5 Immunohistochemistry

The adsorption of PRG4 to collagen-GAG scaffolds was characterized compared to positive cartilage controls (fresh bovine samples). Positive control samples were prepared from fresh articular cartilage discs (mature bovine stifle joints, obtained from a local abattoir in Calgary, AB, Canada under the approval of the Animal Care Committee at the University of Calgary). Samples (labeled as "fresh") were embedded in OCT (Tissue Tek OCT, Sakura, Torrance, CA) and snap-frozen in isopropanol cooled in a liquid nitrogen bath. Collagen-GAG scaffolds were incubated in solutions; PBS (negative control), rhPRG4 @ 450 µg/mL in PBS, and bSF (positive control), overnight at 4°C. Samples were subsequently rinsed in PBS at 4°C overnight, then fixed in OCT and stored at -80°C prior to sectioning.

Sections (10 µm thick) were cut from OCT blocks with a cryostat microtome (CM3050S, Leica Biosystems Concord, Ontario, Canada) and placed onto positively charged glass slides (Super frost Plus Adhesion Slides, Thermo Scientific). Sections were fixed in 4% paraformaldehyde in PBS and washed in PBS to remove OCT. Samples were blocked 10% goat serum with 1% BSA in PBS in a humidity chamber. Samples were incubated overnight in anti-PRG4 monoclonal antibody (mAb) 9G3 (Sigma Aldrich, Oakville, Canada); in 1.5% normal goat serum at a ratio of 1:100. The slides were washed with PBS, and samples were incubated in secondary antibody, Alexa Fluor-594 rhodamine-conjugated goat-anti mouse IgG (Life Technologies, Carlsbad, CA, USA) in 1.5% normal goat serum at a ratio of 1:1000. Finally, the samples were washed with PBS and sealed with microscope coverslips (VWR Scientific Products, PA). Slides were imaged using a Zeiss microscope (Carl Zeiss, Oberkochen, Germany) at a magnification of 10X objective. Fluorescence images were obtained for red (Alexa Fluor-594 rhodamine detected PRG4; excitation/emission of 590/617 nm)

fluorescence, excited by X-Cite 120 (EXFO Photonic Solutions Inc., Mississauga, ON, Canada) and images were captured with an Olympus Camera supplied with DP Controller software.

2.6 Statistical Analysis

For collagen-GAG scaffolds in PBS, the effect of compression (as a repeated factor) on the $F_{N,\ equilibrium}$, τ_Z, and $\mu_{kinetic,\ Neq}$ was assessed by analysis of variance (ANOVA), with Tukey post hoc analysis. The effect of test lubricant groups on $F_{N,\ equilibrium}$, τ_Z, and $\mu_{kinetic,\ Neq}$ at ε=0.2 was assessed by ANOVA, with Tukey post hoc analysis. The effect of test lubricant groups on compressive stiffness (calculated by simple linear regression, SLR) was assessed by analysis of covariance (ANCOVA) to test for differences between regression slopes. The effect of increasing compression on the stress relaxation time constant was assessed by SLR. Unless indicated otherwise, data are presented as the mean ± standard error from the mean, and significance was accepted at a level of $p<0.05$. Statistic analysis was completed with RStudio.

3. **Results**

3.1 Development of a Scaffold-on-Glass Friction Test

3.1.1 *Normal Equilibrium Load ($F_{N,\ equilibrium}$) and Torque (τ_Z) Increase with Compressive Strain*

During boundary mode lubrication of cartilage, fluid is depressurized and the kinetic coefficient of friction ($\mu_{kinetic,\ Neq}$) is invariant over a range of compressive loads. In our scaffold friction test model, $\mu_{kinetic,\ Neq}$ is calculated through the experimental measurement of $F_{N,\ equilibrium}$ and τ_Z. Therefore, as a step towards establishing boundary mode lubrication conditions, we examined the effect of compression on collagen-GAG scaffolds friction tested in PBS solution. $F_{N,\ equilibrium}$ after stress-relaxation increased proportionally with compression strain. $F_{N,\ equilibrium}$ was shown to increase significantly at ε=0.3 (10.6 ± 2.4 mN) compared to ε=0.1 (5.3 ± 1.3 mN, $p<0.05$), at ε=0.4 (14.1 ± 1.7 mN) compared to ε=0.1 ($p<0.001$) and ε=0.2 (8.3 ± 1.0 mN, $p<0.01$), and at ε=0.5 (18.6 ± 4.6 mN) compared to ε=0.1, 0.2 ($p<0.001$) and ε=0.3 ($p<0.01$), see **Fig. 3A**. Similarly, τ_Z was shown to increase proportionally with compression (**Fig. 3C**). A trend towards a significant increase in τ_Z was demonstrated at ε=0.4 (8.7 ± 1.4 mN•mm) compared to ε=0.1 (3.4 ± 0.5, mN•mm, $p=0.06$) and a significant increase was demonstrated at ε=0.5 (10.5 ± 2.2 mN•mm) compared to ε=0.1 ($p<0.001$) and ε=0.2 (4.7 ± 0.85 mN•mm, $p<0.01$) (**Fig. 3B**). τ_Z measurements relate to shear stress and the resistance to articulating motion between the scaffold-glass interface. In the experimental design, compression applied was increased through a sequence of ramps (**Fig. 2**) on each sample, τ_Z increased with compression as expected.

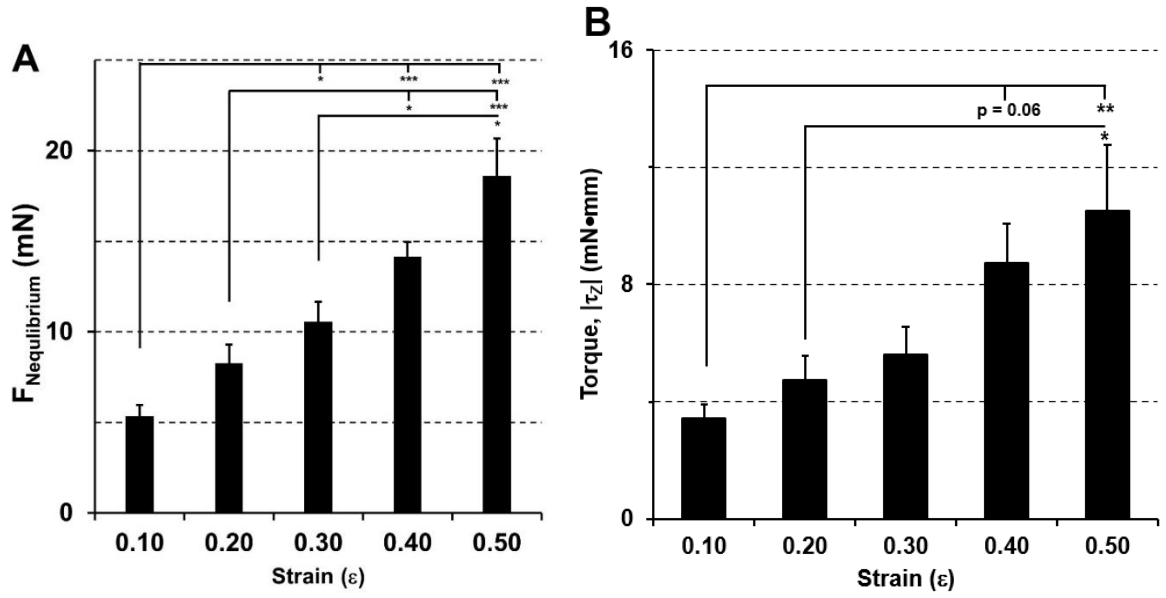
A
B
$F_{Nequilibrium}$ (mN)
Torque, $|\tau_Z|$ (mN•mm)
Strain (ε)
p = 0.06
0.10
0.20
0.30
0.40
0.50
0
10
20
8
16
*
**
***

356

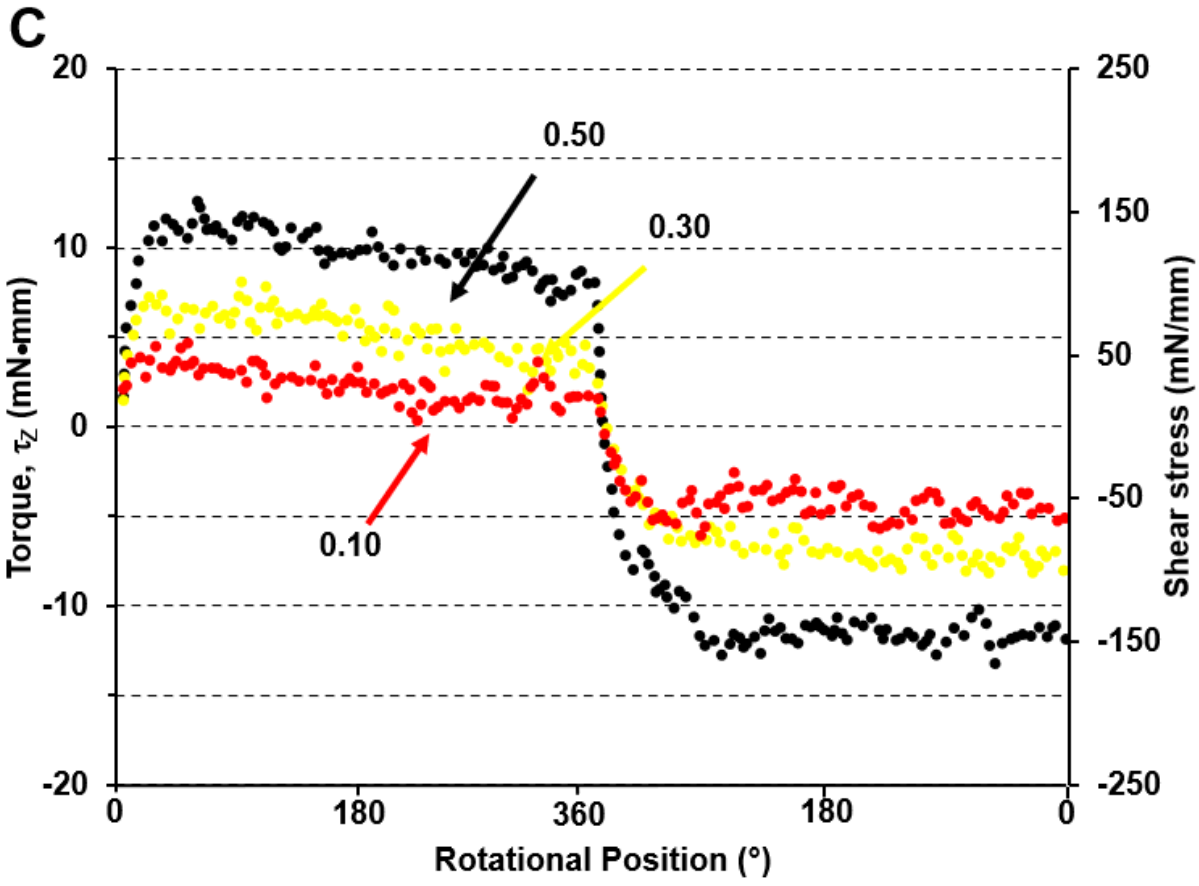
C
Torque, τ_Z (mN•mm)
Shear stress (mN/mm)
Rotational Position (°)
0.50
0.30
0.10
20
10
0
-10
-20
250
150
50
-50
-150
-250
0
180
360

357

Figure 3: (**A**) $F_{N,\ Equilibrium}$ calculated after stress-relaxation across varying compressive strains. (**B**) The absolute torque ($|\tau_Z|$) was calculated from values from positive rotation ($\tau_{Z+,\ 100\text{-}260°}$) and negative rotation as ($\tau_{Z-,\ 260\text{-}100°}$), as $|\tau_Z| = (\tau_{z,+} - \tau_{z,\ -})/2$. (**C**) The torque-rotation profiles with increasing compression are shown as time averaged data (data averaged per second). The secondary vertical axis represents the spatially averaged shear stress determined by the original sample surface area. Select profiles at ε=0.1, 0.3 and 0.5 are shown for clarity. Significance: *p<0.05, **p<0.01, ***p<0.001.

3.1.2 Fluid Depressurization is Observed

We next sought to assess the change in load occurring during scaffold articulation, to ensure stress relaxation/fluid depressurization was complete. In Figure 4B, neither a significant downward slope in force vs. time (indicating ongoing de-pressurization or incomplete sample stress-relaxation), nor significant normal force fluctuations (indicating sample slippage or misalignment during testing) were evident during sample rotation. The stress relaxation duration of ½ minute was sufficient for fluid-depressurization of collagen-GAG scaffolds as shown by flattened force-time slopes (**Fig. 4A**), unchanging normal forces during scaffold articulation (**Fig. 4B**), and the model fit for stress relaxation time constants (**Fig. 4C**). The percent difference in normal force (ΔF_z) from the first and final 10 degrees of rotation was minimal, ranging from 9, 3, 18, 12, and 11%, at a compression of ε=0.1, 0.2, 0.3, 0.4, and 0.5, respectively. The rotation profiles depict the normal force during sample articulation (post-stress relaxation), and a lack of change is indicative that fluid depressurization was complete for materials in this test setup at lower strains (0.1-0.3) (**Fig. 4B**).

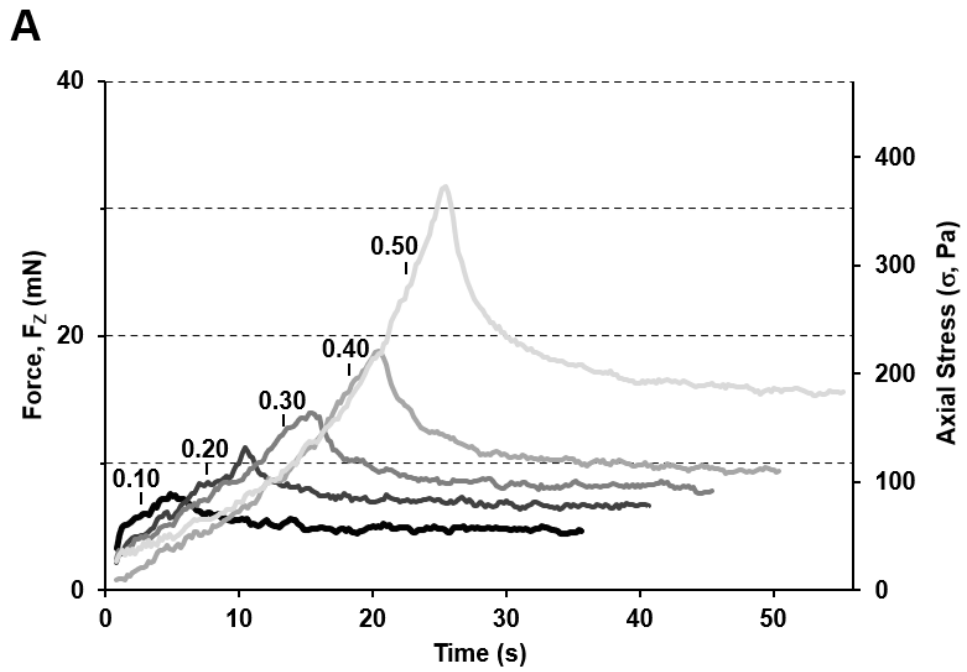
A
40
20
0
Force, F_Z (mN)
400
300
200
100
0
Axial Stress (σ, Pa)
0.50
0.40
0.30
0.20
0.10
0
10
20
30
40
50
Time (s)

380

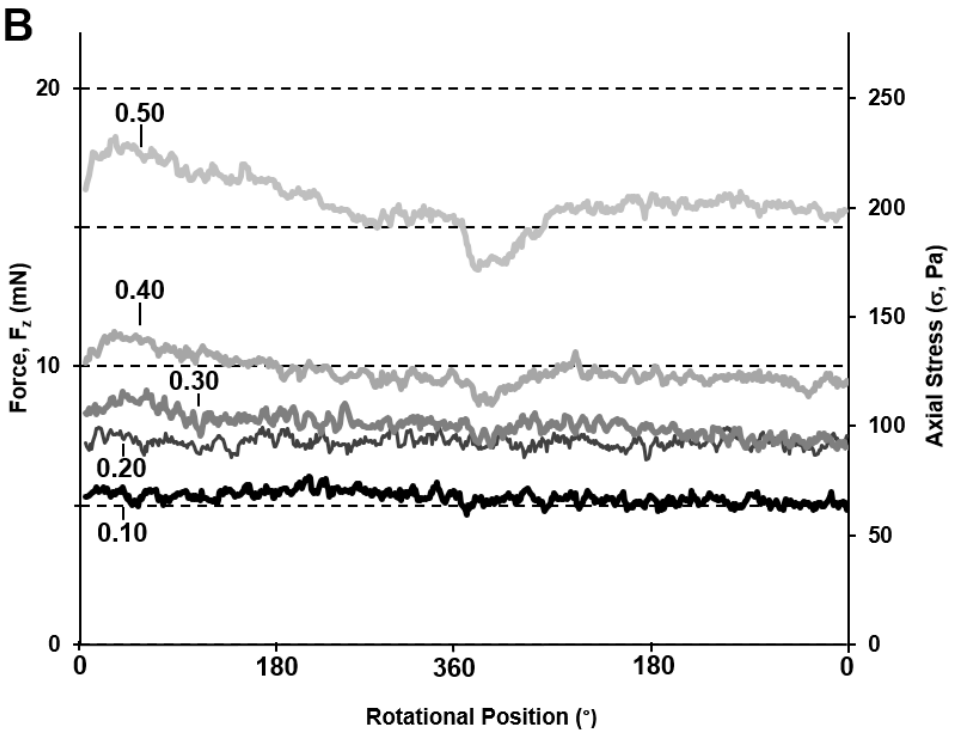
B
20
10
0
Force, F_z (mN)
250
200
150
100
50
0
Axial Stress (σ, Pa)
0.50
0.40
0.30
0.20
0.10
0
180
360
180
0
Rotational Position (°)

381

382

C

ε	$\sigma_{,eq}$ (Pa) ($F_{N,eq}$) (mN)	T	β	R^2
0.10	60.458 (3.430 ± 0.310)	2.826 (1.711 ± 0.223)	0.738 (0.509 ± 0.045)	0.693
0.20	81.327 (5.956 ± 0.406)	1.604 (1.649 ± 0.341)	0.414 (0.606 ± 0.099)	0.750
0.30	102.050 (8.429 ± 0.924)	2.388 (1.640 ± 0.261)	0.572 (0.678 ± 0.053)	0.832
0.40	119.915 (12.559 ± 0.938)	3.119 (2.620 ± 0. 417)	0.667 (0.642 ± 0.049)	0.936
0.50	199.242 (16.409 ± 2.112)	3.277 (3.581 ± 0.771)	0.733 (0.780 ± 0.043)	0.972

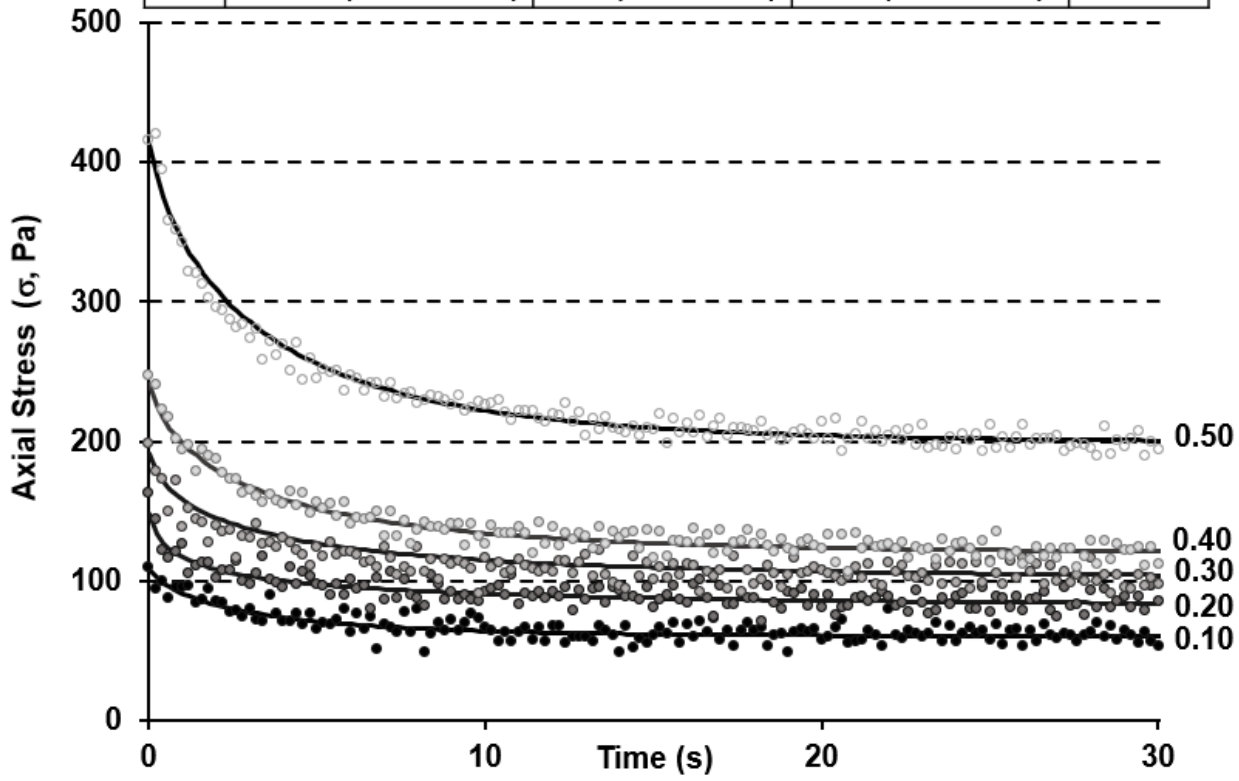

383

384 **Figure 4.** (**A**) Stress-relaxation profiles at increasing compression. (**B**) Force-rotation profiles (F_Z vs.
385 time) during test sequence. The profiles in A and B are shown as time averaged values (data averaged
386 per second). The secondary vertical axis represents an equivalent axial stress, determined by the
387 original sample surface area. (**C**) The stretch relaxation model (**Equation 1**) was fit to normalized
388 stress relaxation data. The model fit to averaged data, model parameters, and data points are shown.
389 The values in brackets represent the model parameters for fits to each experimental run (μ±SEM).
390 Significance; *p<0.05, **p<0.01.

3.1.3 The Conditions for Boundary Mode Lubrication were Established

$\mu_{kinetic,\ Neq}$, of collagen-GAG scaffolds tested in PBS against a glass counterface was invariant (ranging from a low of 0.103 ± 0.010 at ε=0.3 up to 0.121 ± 0.015 at ε=0.4) over increasing compression steps (ε=0.1, 0.2, 0.3, 0.4, and 0.5) ($p>0.05$) (**Fig. 5**). Boundary-mode lubrication (surface to surface contact and minimal fluid film gap) allows for the examination of interactions between synovial fluid lubricants and tissues and has been used for cartilage-cartilage[42] and cartilage-glass studies[43]. Here, $\mu_{kinetic,\ Neq}$ was invariant across a range of compressive strains, indicative of boundary-mode conditions being achieved as expected for a stationary contact rotational set-up. Therefore, the role of synovial lubricants on collagen-GAG scaffold lubrication was examined at ε = 0.2, a strain approximately equivalent to previously reported test parameters (ε = 0.18-0.24[19,42,43]) and when combined with time to allow for fluid depressurization facilitated the study of boundary mode lubrication.

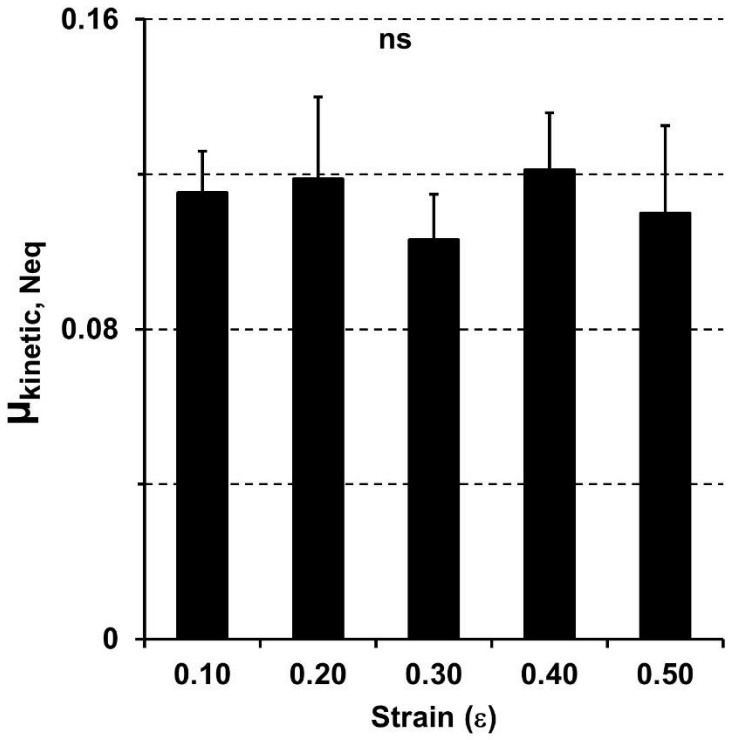

404

405 **Figure 5.** The kinetic coefficient of friction $\mu_{kinetic,\ Neq}$ of collagen-GAG scaffolds articulated against
406 glass in PBS was invariant with increasing compression. Data is presented at μ±SEM, ns: non-
407 significant p>0.05.

408

409 *3.2 The Effect of Synovial Fluid Lubricants on the Frictional Properties of Collagen-GAG Scaffolds*

410 *3.2.1 Immersion of Collagen-GAG Scaffolds in rhPRG4 and HA Does Not Affect $F_{N,\ equilibrium}$ or τ_z*

411 $F_{N,\ equilibrium}$ did not change with test lubricant for collagen-GAG scaffolds (p>0.05) (**Fig. 6A**). $F_{N,}$
412 $_{equilibrium}$ values of collagen-GAG scaffolds tested in lubricants ranged from HA: 7.9 ± 1.6 mN, rhPRG4:
413 9.1 ± 1.2 mN, to bSF: 9.4 ± 2.3 mN (**Fig. 6B**). τ_z measured between the scaffold-glass interface
414 decreased in bSF (2.5 ± 0.7 mN•mm) compared to PBS (4.7 ± 0.9, mN•mm, p<0.05), but not in other
415 lubricants (**Fig. 6 C,D**). This decrease in shear stress (resistance to articulation) observed in normal

bSF indicates a reduction in shear deformation at the surface of compressed scaffolds and would suggest that the permeation of synovial fluid into implanted collagen biomaterials may function to reduce friction.

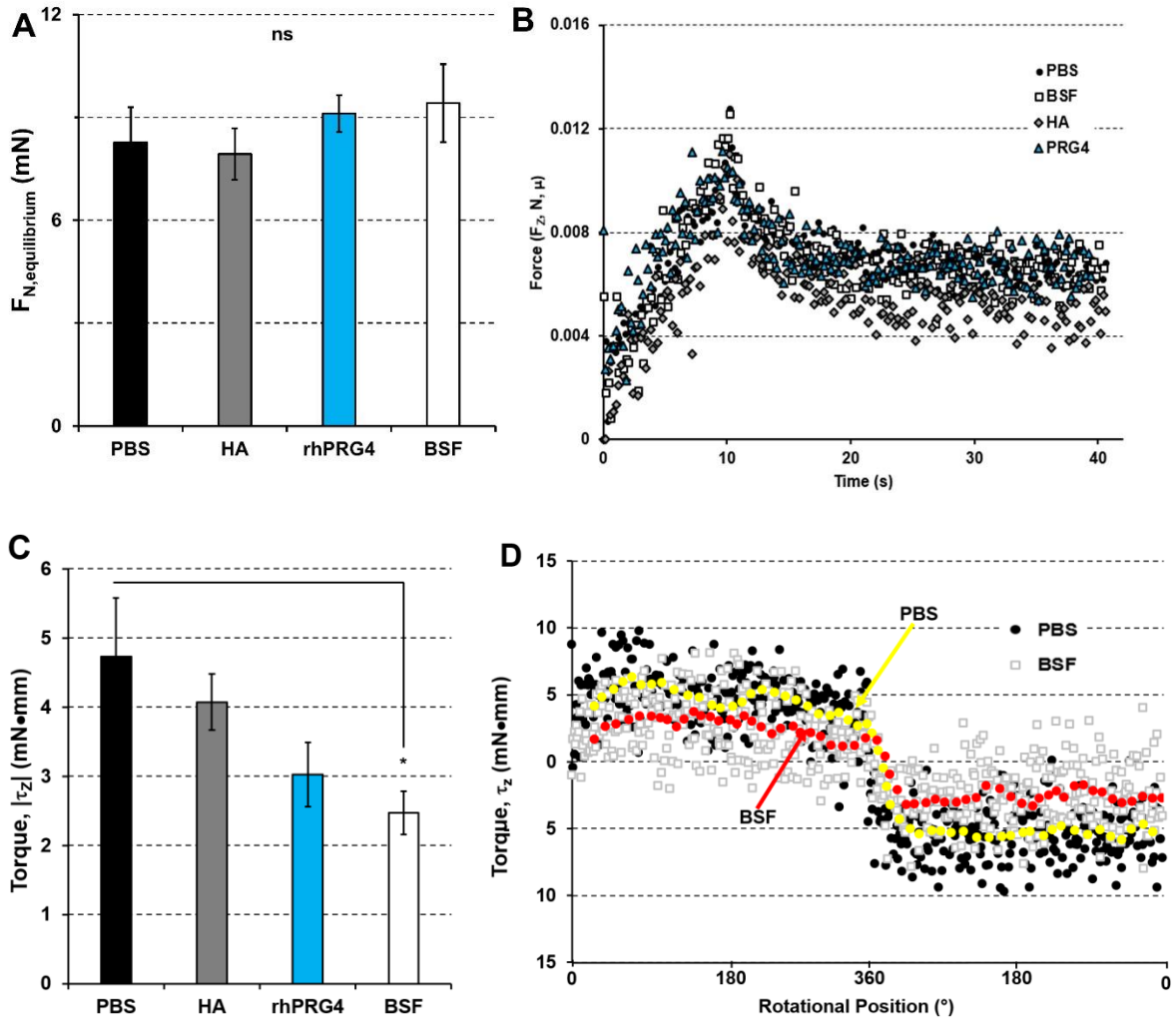

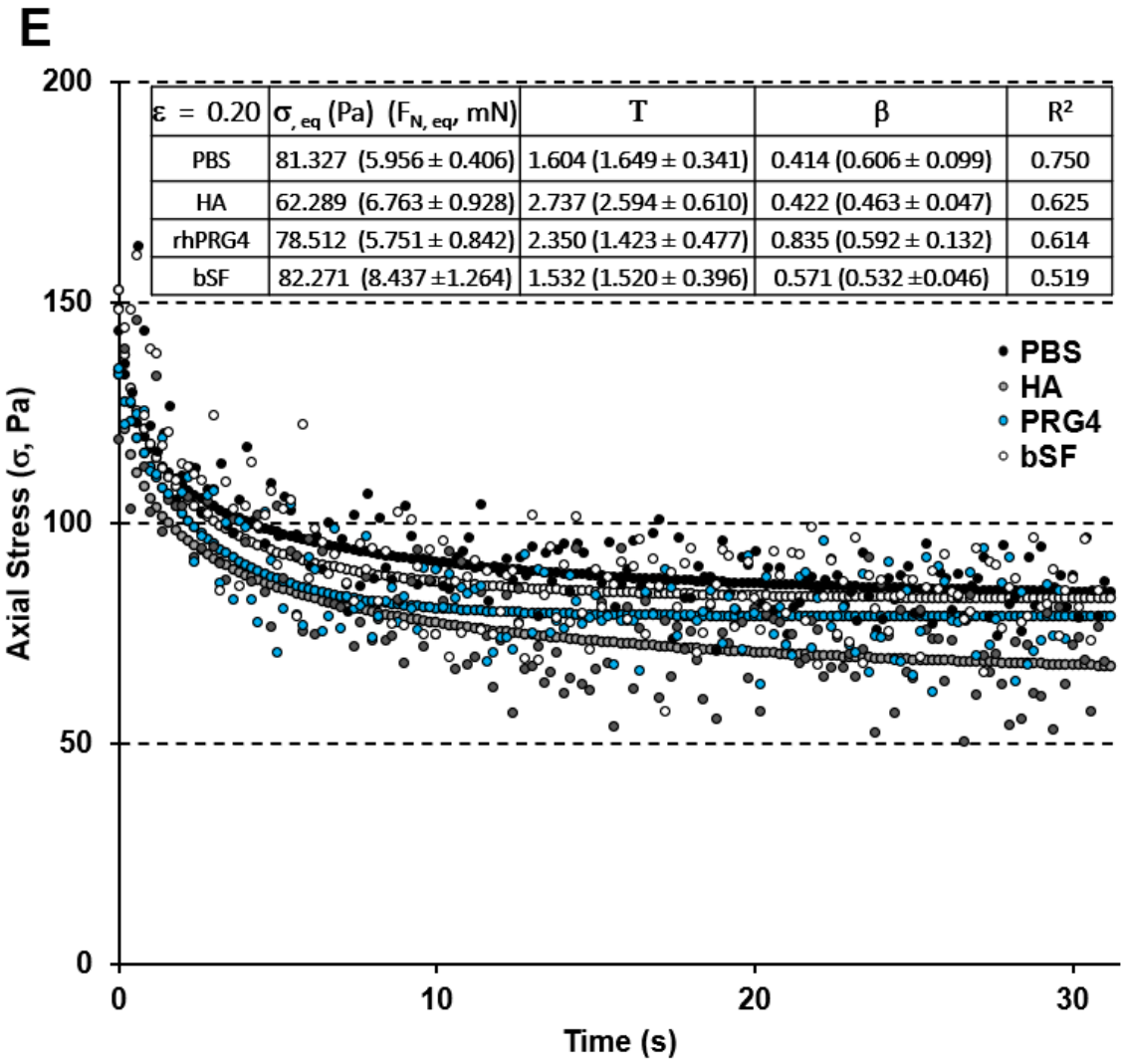

422

423 **Figure 6.** (**A**) $F_{N, equilibrium}$ with ε=0.2 compression and a ½ minute stress-relaxation duration. (**B**) Stress-
424 relaxation profiles of collagen-GAG scaffolds immersed in different lubricants, depicted as mean only
425 for graphical purposes. (**C**) The absolute torque of collagen-GAG scaffolds tested in synovial fluid
426 lubricant. (**D**) Select torque-rotation profiles of collagen-GAG scaffolds tested in bSF and PBS are
427 shown, depicted as mean only, with line of best fit (yellow-PBS, red-bSF) for graphical/visualization
428 purposes. (E) The stretch relaxation model (**Equation 1**) was fit to normalized stress relaxation data.
429 The model fit to averaged data and model parameters are shown. The values in brackets represent

the model parameters for fits to each experimental run (μ±SEM). Significance; *p<0.05, ns: non-significant.

3.2.2. Immersion in rhPRG4 or HA Differentially Regulates the Compressive Stiffness of Collagen-GAG Scaffolds.

The compressive stiffness of collagen-GAG scaffolds significantly decreased in rhPRG4-solution (0.45 ± 0.17 kPa), and significantly increased in both HA and bSF (0.57 ± 0.02 and 0.55 ± 0.02, kPa, respectively), compared to PBS (0.49 ± 0.02 kPa p<0.05) (**Fig. 7A**). The increased stiffness of scaffolds saturated in bSF and HA could perhaps be due to HA entrapment within the porous matrices, preventing the escape of water during compression in a similar fashion to GAGs in cartilage, and swelling to maintain shape. The stress-strain curves of collagen-GAG scaffolds revealed expected compressive responses as described previously[36,35]. There was a linear-elastic response from 0-0.10 strain, followed by a curve in the graph with the onset of pore collapse and struct buckling of collagen-GAG scaffolds (**Fig. 7B**). The properties of collagen-GAG scaffolds did not recover completely with five-minute load removal (indicating permanent deformation to some extent), which is evident with each increasing compression step as the stress response decreases (material softening, the curve is shifted downwards slightly).

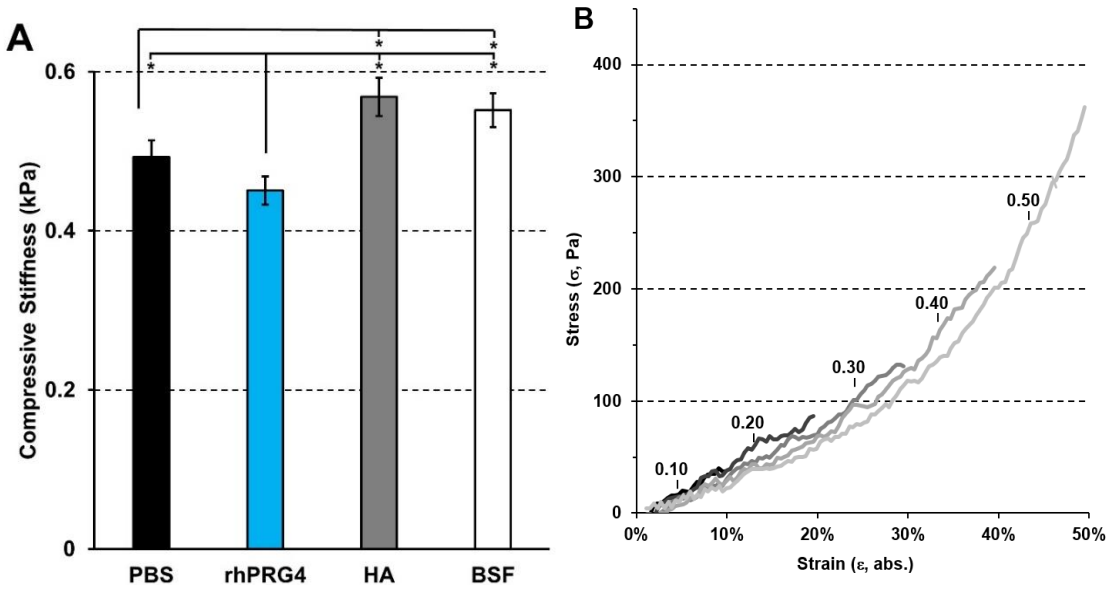

448

449 **Figure 7.** (**A**) The compressive stiffness of collagen scaffolds in synovial fluid lubricants. (**B**) The stress-
450 strain curves of collagen-GAG scaffolds in PBS, shown as time averaged values (data averaged per
451 second). Significance; *p<0.05.

452

453 *3.2.3. Immersion in rhPRG4 Reduces $\mu_{kinetic,\ Neq}$ of Collagen-GAG Scaffolds*

454 $\mu_{kinetic,\ Neq}$ decreased for collagen-GAG scaffolds immersed in rhPRG4-solution (0.067 ± 0.027) and
455 normal bSF (0.056 ± 0.020) compared to PBS (0.118 ± 0.21, both p<0.05) (**Fig. 8**).
456 Immunohistochemistry demonstrated that PRG4 from recombinant human and bovine sources
457 adsorbed onto collagen-GAG scaffolds following a 24-hour incubation in solutions and a subsequent
458 24-hour PBS rinse, prior to specimen processing (**Fig. 9**). Fresh cartilage discs (positive controls)
459 demonstrated a 9G3-immunoreactive layer of native PRG4 localized to the articular surface. PRG4
460 supports cartilage lubrication by domain-specific functions, its C-terminus binds to cartilage
461 surfaces[50], the N-terminal forms disulfide-bonded dimers[51], and the mucin-like middle domain is
462 extensively glycosylated with o-linked oligosaccharides partially capped with sialic acid[44]. Each

domain-specific function contributes to PRG4's lubricity, and in this work, PRG4 adsorption to scaffolds is functional as demonstrated by a reduction in $\mu_{kinetic,\ Neq}$.

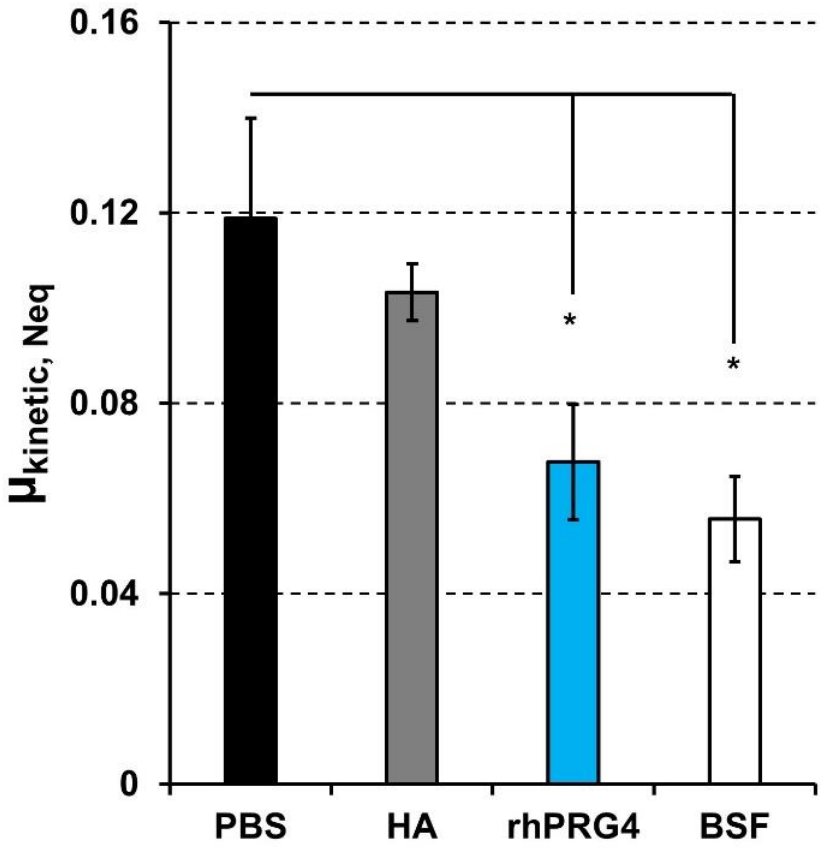

Figure 8. $\mu_{kinetic,\ Neq}$ of collagen-GAG scaffolds immersed in synovial fluid lubricants. Significance *p<0.05.

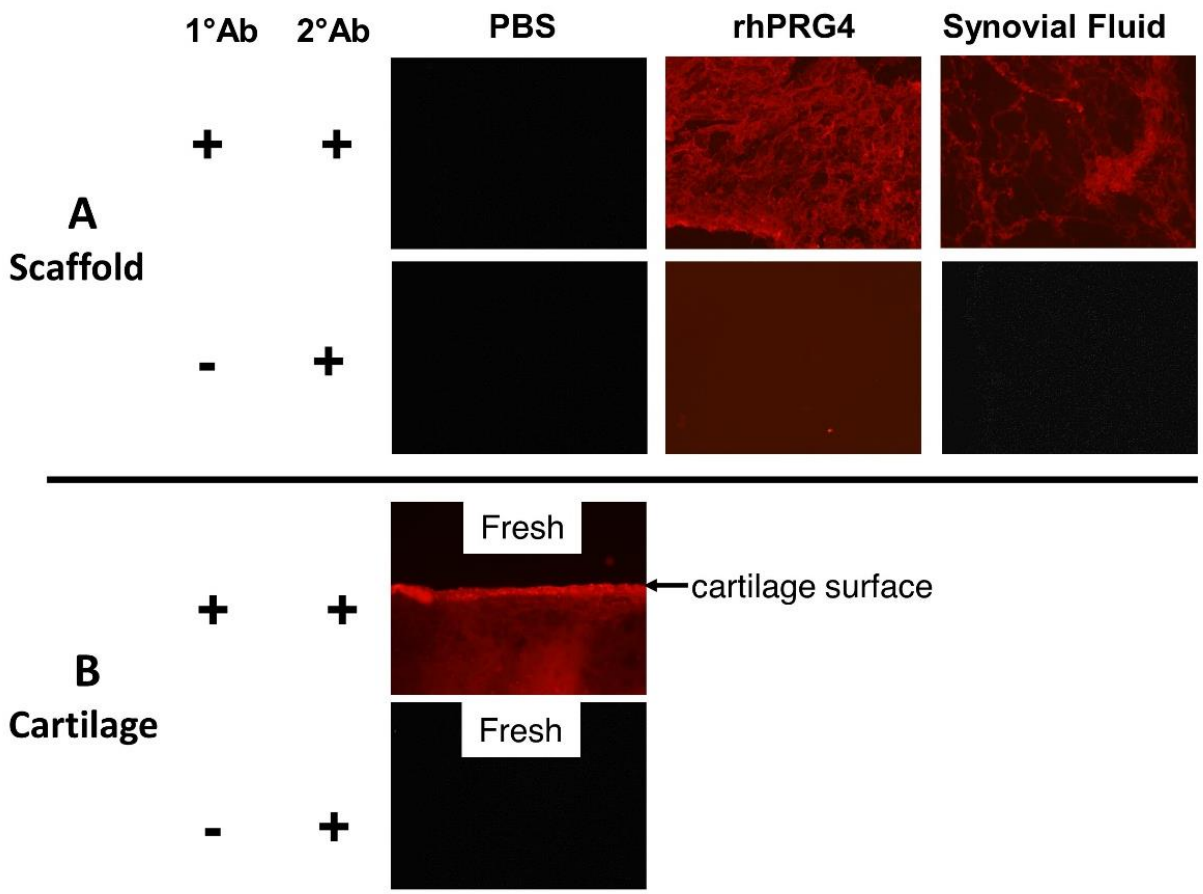

Figure 9. Immunolocalization of PRG4 to fresh articular surfaces – taken directly from joint and snap frozen (positive control). Scaffolds were hydrated in PBS for 1 hour prior to incubation in test solutions overnight (PBS, rhPRG4, bSF). Prior to processing, scaffolds were rinsed in PBS overnight at 4°C. PRG4 adsorbed to cartilage and scaffolds is shown in red.

4. Discussion

The overall objective of this study was to characterize the role of synovial fluid and its constituents on the coefficient of friction of collagen-GAG scaffolds. First, an *in vitro* boundary mode lubrication friction test was developed by characterizing the effect of compressive strain on the kinetic coefficient of friction of collagen-GAG scaffolds. Subsequently, this setup was used to determine the role of physiological lubricants on the frictional properties of collagen-GAG scaffolds. The results described here indicate that a stationary rotational test configuration may be useful for elucidating the lubricating-ability of ECM-derived scaffolds against a glass interface. In PBS, both $F_{N,\ equilibrium}$ during stress relaxation and τ_z during rotation increased proportionally with increasing compressive strain. The stress relaxation duration of ½ minute was appropriate for fluid-depressurization of collagen-GAG scaffolds at all strains (0.1-0.5), time constants for relaxation were determined by fitting data to a stretch exponential model. The coefficient of friction for collagen-GAG scaffolds in PBS was invariant across the compressive strains examined here, thus establishing boundary mode lubrication test conditions. Friction for collagen-GAG scaffolds tested in rhPRG4-solution and bSF decreased compared to PBS. Interestingly, PRG4 (from both recombinant human and bovine sources) adsorbed to collagen-GAG scaffolds. These results suggest rhPRG4 in solution adsorbs onto collagen-GAG scaffolds in a functionally determinant manner, which improves the lubricity of scaffolds, and highlights its capacity to augment the frictional properties of collagen-based biomaterials for cartilage repair.

The proportional increases of both normal equilibrium force and torque resulted in constant friction of collagen scaffolds in PBS across the compressive strains assessed. The normal equilibrium force

500 of collagen-GAG scaffolds in PBS increased proportionally with increasing compressive strain.
501 Stress-strain profiles showed responses characteristic for collagen-GAG scaffolds, with a linear
502 response at low strains (up to $\varepsilon = 0.1$) followed by a curved response due to the onset of pore strut
503 buckling and pore-collapse at higher strains (0.2-0.5). Experimentally fit model time constants
504 demonstrated that for all strains tested (0.1-0.5), stress-relaxation was complete at ½ minute. In a
505 comparable friction test study by Gleghorn *et al.* 2010[34], (examining stiffer porous polyurethane
506 foams as cartilage replacements), stress relaxation data were fit to a biphasic model. The time
507 constants reported were approximately 10s at $\varepsilon = 0.30$, 15s at $\varepsilon = 0.4$, and 60s at $\varepsilon = 0.5$, with the
508 recommendation that stress-relaxation durations should be four times the stress-relaxation time
509 constant. In the present study, nonlinear fitting to the stretch relaxation model (described by June
510 *et al*, 2009[47] and June *et al*, 2013[46]) demonstrated smaller time constants for biomaterials studied in
511 this work. Smaller time constants would be expected for the relative soft scaffolds with high
512 porosity (>98%)[27] (and therefore permeability), allowing fluid flow and faster depressurization. The
513 time constants for collagen-GAG scaffolds in PBS gradually increased with compression (SLR,
514 $p<0.01$, adjusted $R^2=0.265$) which was comparable to findings in previous cartilage work[48]. The
515 parameter β represents the width of the relaxation-time distribution ($0 < \beta < 1$). Physically, β is
516 associated with the polymer motion known as reptation. The polymer reptation dynamics applies to
517 the stretch relaxation response of native cartilage[52], and biopolymers (chondroitin sulfate,
518 proteoglycan, hyaluronan) have essential roles, although the individual contribution by each has not
519 been examined. Hyaluronan alone has a more significant role in cartilage polymer dynamics than its
520 side chains or attached proteoglycans[52]. In addition, smaller stretching exponent parameters are
521 associated with cartilage deterioration[52], and enzymatic digestion of cartilage components[47]. In this
522 work, the stretch ratio was consistent for scaffolds in PBS at various compressions and in various

lubricants. In the present study, torque also increased with compressive strain, possibly as scaffold pores and the overall structure flattened, increasing the surface area of the scaffold in contact with the glass and adding additional resistance during rotation. Higher compression (>0.1) may be suitable to examine surface interactions and possibly the role of bound or interacting synovial fluid lubricants on the lubricating ability of collagen-GAG scaffolds. Therefore, to determine the role of synovial fluid constituents on the lubricating ability collagen-GAG scaffolds, a compressive strain of 0.2 was selected to ensure complete fluid depressurization and full-contact between interfaces.

The ability of rhPRG4 and bSF to lubricate collagen-scaffolds is consistent with previous studies at cartilage-glass[53], latex-glass[54], and cartilage–cartilage[19] interfaces. In the present work, collagen-GAG scaffolds lubricated by either rhPRG4 solution or bSF decreased friction efficiently at low speed against a glass surface. Native PRG4 binds to cartilage surfaces by its C-terminal domain[50] and via binding partners (cartilage oligomeric protein (COMP), fibronectin, and collagen II)[55], to collagen II *in vitro*[56], and to collagen IV[57]. In this study, rhPRG4 in solution absorbed to collagen-GAG scaffolds in a functional manner to reduce friction. The terminal domain(s) of native PRG4 bind to cartilage surfaces, and its negatively charged mucin domain extends outward to form an aqueous film covering which lowers friction against the opposing contact-surface. Therefore, given the reduction of friction observed with bSF as a lubricant, it follows that PRG4 in bSF possibly adhered to collagen-GAG scaffolds in a similar manner. Quantifying PRG4 (rh/bSF) adherence to collagen-GAG scaffolds (number and manner of binding), as previously done for cartilage samples[58], could be completed in future work. PRG4 is present within the superficial layer of cartilage, and attached to its surface where it is critical in the maintenance of low friction between apposed sliding surfaces[54] within the body. The addition of PRG4 to tissue-engineered scaffolds may optimize the frictional properties of these

546 constructs for *in-vivo* use. For example, in contact lens biomaterials, the comfort of use was
547 previously optimized with the addition of PRG4 to improve surface wettability[59] and reduce surface
548 friction[60,61]. HA-solution did not modulate the lubricating ability compared to PBS. It has been
549 postulated that PRG4 at the surface of cartilage anchors HA close to the surface where it acts as a
550 boundary lubricant[53]. According to this theory, without PRG4 at the surface, HA-solution alone cannot
551 support boundary lubrication. However, in similar experimental work by Abubacker *et al.* 2018, HA-
552 solution supported lubrication at cartilage-cartilage interfaces but failed to lubricate cartilage-glass
553 interfaces[43]. These findings suggest that friction test counterfaces may impact reported findings, and
554 the use of glass may not be suitable to examine the role of HA in boundary lubrication. Still, collagen-
555 GAG scaffolds may be useful materials to examine the interactions of physiological lubricants more
556 closely, and further studies could extend to examine a combination of solutions on the lubricating
557 ability of collagen scaffolds, including for example rhPRG4 + HA.

558

559 Collagen scaffolds may also be suitable substrates to elucidate the contributions of individual
560 components to the mechanical properties of cartilage via a bottom-up methodology. Previous works
561 have examined the mechanical properties of cartilage, including compressive stiffness, dynamic shear
562 stiffness, and lubricating ability through top-down approaches. In these methods, select elements of
563 cartilage are digested followed by characterization of the effect to *in vitro* biomechanics. Cartilage
564 compressive stiffness deteriorates with solid matrix and proteoglycan degradation[62,63,64], the dynamic
565 shear stiffness decreases with proteoglycan-depletion, collagen degradation, and the removal of
566 chondroitin and hyaluronan[65], and the surface friction of proteoglycan-depleted[19,66] cartilage plugs is
567 significantly increased. In the present study, the addition of synovial fluid lubricants modulated
568 compressive stiffness and lubricating ability. Immersing collagen-GAG scaffolds in bSF and HA-

569 solution increased compressive stiffness, possibly by hydration (via HA) and swelling, to allow
570 collagen-GAG scaffolds to retain shape and resist deformation, as occurs in native cartilage. However,
571 the direct measurement of solution osmolarity would be necessary to clarify this affect. In rhPRG4
572 solution, the compressive stiffness **(Fig. 7A)** of scaffolds was decreased, possibly owing to solution
573 viscosity and a faster exudation of fluid from materials. The effect of test lubricant viscosity on the
574 compressive stiffness of scaffolds was transient. After strain was applied and stress relaxation
575 occurred, the equilibrium axial loads were not different between lubricants (**Fig. 6AB**). Previously,
576 disparate effects of PRG4 to solution viscosity have been reported, PRG4 decreases the dynamic
577 viscosity of solutions[67] and others reported increased viscosity (resistance to diffusion) with its
578 addition[68]. Therefore, it remains to be clarified if PRG4 may contribute to the mechanical properties
579 of other biological tissues beyond enhanced lubrication, how transient or equilibrium properties are
580 affected, and how PRG4 may decrease (or enhance) mechanical stiffness. It should also be noted that
581 the scaling-up of these ECM-derived biomaterials to treat large defects, or even to resurface entire
582 condyles, would likely require the generation of scaffolds with additional mechanical reinforcement.
583 In this regard, additive manufacturing techniques, such as those recently leveraged to reinforce
584 cartilaginous templates for osteochondral repair with 3D printed polymer frames[69], could potentially
585 be applied.

586

587 This study was not without limitations, including the use of a non-physiological scaffold-on-glass
588 interface (stationary contact, rotational setup). The friction-test interface lacks certain surface
589 characteristics and may not accurately mimic naturally articulating surfaces, where molecular
590 interactions between surface and lubricants are important and operative to articulation[19,42].
591 However, it should be noted that glass interfaces have been used extensively to characterize the

592 frictional properties of tissue-engineered cartilage[70,71], orthopedic implants[72], the role of synovial
593 fluid lubricants[53,43], and the role of cartilage[73,74,75,76] and in this study was used to successfully
594 distinguish the difference between negative (PBS) and positive (bSF) control lubricants for collagen-
595 GAG scaffolds. In addition, although the objective was to examine the effect of compressive strain,
596 the effect of sliding velocity and stress-relaxation was excluded. The sliding velocity used was slow
597 and constant for all tests completed, important in establishing boundary mode lubrication
598 conditions[42]. In addition, porous-collagen scaffolds exhibit rate-dependent tensile responses[37], and
599 at higher velocities surface shear deformation is significant causing samples to dislodge from setup
600 and adding significant variability between tests. Although not explicitly examined (e.g., by video
601 capture), sample slippage or misalignment between at the sample-sandpaper interface was not
602 evident with the test's slow sliding velocity, the low torques measured, and the strength of glue.
603 During rotation, normal forces (Fig. 4B) and torque (Fig. 3C) were generally constant and scaffolds
604 remained in position; therefore, if any slippage and/or misalignment occurred, they (and their
605 effects) would have been minimal. The stress-relaxation duration of ½ minute was selected during
606 pilot studies at $\varepsilon = 0.3$, where stress-relaxation slopes of 0.01 N/min were evident at 30s. Finally, the
607 kinetic coefficient of friction of scaffolds was calculated using the outer scaffold radius. This
608 calculation does not account for velocity and torque variation with radius, approximately zero at the
609 center of to a maximum along the outer radius. Therefore, while magnitude of the calculated friction
610 coefficient is affected by this fact, the calculated coefficient of friction is still suitable as an average
611 friction value for comparison between groups in this study.

612

613 In conclusion, the effect of compressive strain and the role of synovial fluid lubricants on the
614 coefficient of friction of collagen-based scaffolds was characterized. The coefficient of friction of

scaffolds in PBS was invariant across increasing compressive strain steps tested here, indicative of boundary-mode lubrication conditions. Encouragingly, both bSF and rhPRG4-solution reduced friction of collagen-GAG scaffolds against a glass interface. These data collectively point to the importance of frictional properties as modifiable design parameters for implants and materials for soft tissue replacement. Lastly, rhPRG4 adsorbed to collagen-GAG scaffolds in a conformation that enhanced material lubricity against a glass interface. It follows, therefore, that the incorporation of rhPRG4 within collagen-GAG scaffolds may enhance the lubricating ability of tissue-engineered cartilage replacements.

5. Acknowledgments

This work was funded in part by the University of Calgary Biomedical Engineering Graduate Program (AM), the University of Calgary Faculty of Veterinary Medicine (MS), the European Research Council under the European Community's Horizon 2020 research and innovation programme under ERC grant agreement no. 788753 (ReCaP) (FO), the EU BlueHuman Interreg Atlantic Area Project (EAPA_151/2016) (ES, FO), and the Department of Biomedical Engineering at the University of Connecticut Health Center (TS). Study conception and design was completed by AM, ES and TS. Acquisition of data was performed by AM (friction test method development and execution) and ES (collagen-GAG scaffold production). All others were involved in analysis and interpretation of data. Original draft preparation of the article was performed by AM and ES. All authors were involved in revising the article. The authors are grateful to Professor Leping Li for providing expertise and helpful suggestions with biomechanical modeling. The authors also thank Lμbris Biopharma for providing recombinant human proteoglycan-4.

637

638 **Disclosure Statement**

639 Dr. Jay and Dr. Schmidt own equity in Lμbris BioPharma and have licensed patents related to the use of

640 rhPRG4. Dr. Schmidt also consults for Lμbris BioPharma.

641

642

6. References

1. Langer R. 2000. Tissue Engineering. Mol. Ther. 1(1):12–15 Available from: http://dx.doi.org/10.1006/mthe.1999.0003.

2. O'Brien FJ. 2011. Biomaterials and scaffolds for tissue engineering. Mater. Today 14(3).

3. Lee CR, Grodzinsky AJ, Spector M. 2001. The effects of cross-linking of collagen-glycosaminoglycan scaffolds on compressive stiffness, chondrocyte-mediated contraction, proliferation and biosynthesis. Biomaterials 22(23):3145–3154.

4. Vickers SM, Squitieri LS, Spector M. 2006. Effects of cross-linking type II collagen-GAG scaffolds on chondrogenesis in vitro: dynamic pore reduction promotes cartilage formation. Tissue Eng. 12(5):1345–1355.

5. Patel JM, Wise BC, Bonnevie ED, Mauck RL. 2019. A Systematic Review and Guide to Mechanical Testing for Articular Cartilage Tissue Engineering. Tissue Eng. Part C Methods 25(10):593–608 Available from: https://doi.org/10.1089/ten.tec.2019.0116.

6. Northwood E, Fisher J. 2007. A multi-directional in vitro investigation into friction, damage and wear of innovative chondroplasty materials against articular cartilage. Clin. Biomech. (Bristol, Avon) 22(7):834–842.

7. Gleghorn JP, Jones ARC, Flannery CR, Bonassar LJ. 2007. Boundary mode frictional properties of engineered cartilaginous tissues. Eur. Cell. Mater. 14:20–29.

8. Northwood E, Fisher J, Kowalski R. 2007. Investigation of the friction and surface degradation of innovative chondroplasty materials against articular cartilage. Proc. Inst. Mech. Eng. H. 221:263–279.

9. Higginson GR, Norman R. 1974. A model investigation of squeeze-film lubrication in animal joints. Phys. Med. Biol. 19(6):785–792.

10. Walker PS, Dowson D, Longfield MD, Wright V. 1968. "Boosted lubrication" in synovial joints by fluid entrapment and enrichment. Ann. Rheum. Dis. 27(6):512–520 Available from: https://pubmed.ncbi.nlm.nih.gov/5728097.

11. Mcutchen CW. 1966. Boundary lubrication by synovial fluid: demonstration and possible osmotic explanation. Fed. Proc. 25(3):1061–1068.

12. Lewis PR, McCutchen CW. 1959. Experimental evidence for weeping lubrication in mammalian joints. Nature 184:1285.

13. Linn FC. 1968. Lubrication of animal joints. II. The mechanisms. J. Biomech. 1:193–205.

14. Wright V, Dowson D. 1976. Lubrication and cartilage. J. Anat. 121(Pt 1):107–118 Available from: http://www.ncbi.nlm.nih.gov/pmc/articles/PMC1231823/.

15. Gleghorn JP, Bonassar LJ. 2008. Lubrication mode analysis of articular cartilage using Stribeck surfaces. J. Biomech. 41(9):1910–1918 Available from:

https://www.ncbi.nlm.nih.gov/pubmed/18502429.

16. Krishnan R, Kopacz M, Ateshian GA. 2004. Experimental verification of the role of interstitial fluid pressurization in cartilage lubrication. J. Orthop. Res. 22(3):565–570.

17. Bonnevie ED, Baro V, Wang L, Burris DL. 2011. In-situ studies of cartilage microtribology: roles of speed and contact area. Tribol. Lett. 41(1):83–95 Available from: https://pubmed.ncbi.nlm.nih.gov/21765622.

18. Caligaris M, Ateshian GA. 2008. Effects of sustained interstitial fluid pressurization under migrating contact area, and boundary lubrication by synovial fluid, on cartilage friction. Osteoarthr. Cartil. 16(10):1220–1227 Available from: https://pubmed.ncbi.nlm.nih.gov/18395475.

19. Schmidt TA, Gastelum NS, Nguyen QT, et al. 2007. Boundary lubrication of articular cartilage: Role of synovial fluid constituents. Arthritis Rheum. 56(3):882–891.

20. Smith DW, Gardiner BS, Zhang L, Grodzinsky AJ. 2019. Articular Cartilage Dynamics. Signapore: Springer Nature. 333 p.

21. Ludwig TE, Hunter MM, Schmidt TA. 2015. Cartilage boundary lubrication synergism is mediated by hyaluronan concentration and PRG4 concentration and structure. BMC Musculoskelet. Disord. 16(1):386 Available from: http://www.pubmedcentral.nih.gov/articlerender.fcgi?artid=4678696&tool=pmcentrez&rendertype=abstract.

22. Waller KA, Zhang LX, Elsaid KA, et al. 2013. Role of lubricin and boundary lubrication in the prevention of chondrocyte apoptosis. Proc. Natl. Acad. Sci. U. S. A. 110(15):5852–5857 Available from: https://www.ncbi.nlm.nih.gov/pubmed/23530215.

23. Waller KA, Zhang LX, Fleming BC, Jay GD. 2012. Preventing friction-induced chondrocyte apoptosis: comparison of human synovial fluid and hylan G-F 20. J. Rheumatol. 39(7):1473–1480.

24. Bonnevie E, Delco M, Bartell L, et al. 2018. Microscale Frictional Strains Determine Chondrocyte Fate in Loaded Cartilage. J. Biomech. 74.

25. Sheehy EJ, Cunniffe GM, O'Brien FJ. 2018. Collagen-based biomaterials for tissue regeneration and repair. In: In Peptides and Proteins as Biomaterials for Tissue Regeneration and Repair. Woodhead Publishing. p 127–150 Available from: http://www.sciencedirect.com/science/article/pii/B978008100803400005X.

26. Farrell E, O'Brien FJ, Doyle P, et al. 2006. A collagen-glycosaminoglycan scaffold supports adult rat mesenchymal stem cell differentiation along osteogenic and chondrogenic routes. Tissue Eng. 12(3):459–468.

27. Matsiko A, Levingstone TJ, O'Brien FJ, Gleeson JP. 2012. Addition of hyaluronic acid improves cellular infiltration and promotes early-stage chondrogenesis in a collagen-based scaffold for cartilage tissue engineering. J. Mech. Behav. Biomed. Mater. 11:41–52.

28. do Amaral RJ, Matsiko A, Tomazette MR, et al. 2015. Platelet-rich plasma releasate differently stimulates cellular commitment toward the chondrogenic lineage according to concentration. J. Tissue Eng. 6:2041731415594127.

29. Almeida H V, Liu Y, Cunniffe GM, et al. 2014. Controlled release of transforming growth factor-beta3 from cartilage-extra-cellular-matrix-derived scaffolds to promote chondrogenesis of human-joint-tissue-derived stem cells. Acta Biomater. 10(10):4400–4409.

30. Matsiko A, Levingstone TJ, Gleeson JP, O'Brien FJ. 2015. Incorporation of TGF-beta 3 within collagen-hyaluronic acid scaffolds improves their chondrogenic potential. Adv. Healthc. Mater. 4(8):1175–1179.

31. Levingstone TJ, Thompson E, Matsiko A, et al. 2016. Multi-layered collagen-based scaffolds for osteochondral defect repair in rabbits. Acta Biomater. 32:149–160.

32. Levingstone TJ, Ramesh A, Brady RT, et al. 2016. Cell-free multi-layered collagen-based scaffolds demonstrate layer specific regeneration of functional osteochondral tissue in caprine joints. Biomaterials 87:69–81 Available from: http://www.sciencedirect.com/science/article/pii/S0142961216001113.

33. Stack JD, Levingstone TJ, Lalor W, et al. 2017. Repair of large osteochondritis dissecans lesions using a novel multilayered tissue engineered construct in an equine athlete. J. Tissue Eng. Regen. Med. 11(10):2785–2795.

34. Gleghorn JP, Doty SB, Warren RF, et al. 2010. Analysis of frictional behavior and changes in morphology resulting from cartilage articulation with porous polyurethane foams. J. Orthop. Res. 28(10):1292–1299 Available from: https://doi.org/10.1002/jor.21136.

35. Gibson L, Ashbey M. 1999. The mechanics of foams: basic results. In: Cellular Solids: Structure and Properties, 2nd ed. Cambridge University Press. p 510.

36. Harley BA, Leung JH, Silva ECCM, Gibson LJ. 2007. Mechanical characterization of collagen-glycosaminoglycan scaffolds. Acta Biomater. 3(4):463–474.

37. Roeder BA, Kokini K, Sturgis JE, et al. 2002. Tensile mechanical properties of three-dimensional type I collagen extracellular matrices with variedmicrostruture. J. Biomech. Eng. 124(2):214–222.

38. Gleeson JP, Levingstone, Tanya J. O'Brien FJ. 2015. Layered collagen and HA scaffold suitable for osteochondral repair.

39. O'Brien FJ, Harley BA, Yannas I V, Gibson L. 2004. Influence of freezing rate on pore structure in freeze-dried collagen-GAG scaffolds. Biomaterials 25(6):1077–1086.

40. Haugh MG, Murphy CM, O'Brien FJ. 2010. Novel freeze-drying methods to produce a range of collagen-glycosaminoglycan scaffolds with tailored mean pore sizes. Tissue Eng. Part C. Methods 16(5):887–894.

41. Waller KA, Chin KE, Jay GD, et al. 2017. Intra-articular Recombinant Human Proteoglycan

4 Mitigates Cartilage Damage After Destabilization of the Medial Meniscus in the Yucatan Minipig. Am. J. Sports Med. 45(7):1512–1521.

42. Schmidt TA, Sah RL. 2007. Effect of synovial fluid on boundary lubrication of articular cartilage. Osteoarthr. Cartil. 15(1):35–47.

43. Abubacker S, McPeak A, Dorosz SG, et al. 2018. Effect of counterface on cartilage boundary lubricating ability by proteoglycan 4 and hyaluronan: Cartilage-glass versus cartilage-cartilage. J. Orthop. Res. 36(11):2923–2931 Available from: https://www.ncbi.nlm.nih.gov/pubmed/29978918.

44. Jay GD, Harris DA, Cha CJ. 2001. Boundary lubrication by lubricin is mediated by O-linked beta(1-3)Gal-GalNAc oligosaccharides. Glycoconj. J. 18(10):807–815.

45. June RK, Neu CP, Barone JR, Fyhrie DP. 2011. Polymer Mechanics as a Model for Short-Term and Flow-Independent Cartilage Viscoelasticity. Mater. Sci. Eng. C. Mater. Biol. Appl. 31(4):781–788 Available from: https://pubmed.ncbi.nlm.nih.gov/21552375.

46. June RK, Fyhrie DP. 2013. A comparison of cartilage stress-relaxation models in unconfined compression: QLV and stretched exponential in combination with fluid flow. Comput. Methods Biomech. Biomed. Engin. 16(5):565–576.

47. June RK, Fyhrie DP. 2009. Enzymatic digestion of articular cartilage results in viscoelasticity changes that are consistent with polymer dynamics mechanisms. Biomed. Eng. Online 8(1):32 Available from: https://doi.org/10.1186/1475-925X-8-32.

48. June RK, Ly S, Fyhrie DP. 2009. Cartilage stress-relaxation proceeds slower at higher compressive strains. Arch. Biochem. Biophys. 483(1):75–80.

49. Jutila AA, Zignego DL, Schell WJ, June RK. 2015. Encapsulation of Chondrocytes in High-Stiffness Agarose Microenvironments for In Vitro Modeling of Osteoarthritis Mechanotransduction. Ann. Biomed. Eng. 43(5):1132–1144 Available from: https://doi.org/10.1007/s10439-014-1183-5.

50. Jones A, Gleghorn J, Hughes C, et al. 2007. Binding and localization of recombinant Lubricin to articular cartilage surfaces. J. Orthop. Res. 25:283–292.

51. Abubacker S, Ponjevic D, Ham HO, et al. 2016. Effect of disulfide bonding and multimerization on proteoglycan 4's cartilage boundary lubricating ability and adsorption. Connect. Tissue Res. 57(2):113–123.

52. Fyhrie DP, Barone JR. 2003. Polymer Dynamics as a Mechanistic Model for the Flow-Independent Viscoelasticity of Cartilage . J. Biomech. Eng. 125(5):578–584 Available from: https://doi.org/10.1115/1.1610019.

53. Bonnevie ED, Galesso D, Secchieri C, et al. 2015. Elastoviscous Transitions of Articular Cartilage Reveal a Mechanism of Synergy between Lubricin and Hyaluronic Acid. PLoS One 10(11):e0143415–e0143415 Available from: https://www.ncbi.nlm.nih.gov/pubmed/26599797.

54. Jay GD. 1992. Characterization of a bovine synovial fluid lubricating factor. I. Chemical, Surface activity and lubricating properties. Connect. Tissue Res. 28(1–2).

55. Flowers SA, Zieba A, Örnros J, et al. 2017. Lubricin binds cartilage proteins, cartilage oligomeric matrix protein, fibronectin and collagen II at the cartilage surface. Sci. Rep. 7(1):13149 Available from: https://www.ncbi.nlm.nih.gov/pubmed/29030641.

56. Chang DP, Guilak F, Jay GD, Zauscher S. 2014. Interaction of lubricin with type II collagen surfaces: adsorption, friction, and normal forces. J. Biomech. 47(3):659–666 Available from: https://pubmed.ncbi.nlm.nih.gov/24406099.

57. Flannery CR, Yang Z, Zeng W, et al. 2010. Proteomic identification of novel lubricin-binding ligands at cartilage surfaces. Trans. Orthop. Res. Soc. (164):20170.

58. Abubacker S, Dorosz SG, Ponjevic D, et al. 2016. Full-Length Recombinant Human Proteoglycan 4 Interacts with Hyaluronan to Provide Cartilage Boundary Lubrication. Ann. Biomed. Eng. 44(4):1128–1137.

59. Subbaraman LN, Schmidt TA, Sheardown H. 2012. Proteoglycan 4 (lubricin) Enhances the Wettability Of Model Conventional And Silicone Hydrogel Contact Lenses. Invest. Ophthalmol. Vis. Sci. 53(14):6097.

60. Korogiannaki M, Samsom M, Schmidt TA, Sheardown H. 2018. Surface-Functionalized Model Contact Lenses with a Bioinspired Proteoglycan 4 (PRG4)-Grafted Layer. ACS Appl. Mater. Interfaces 10(36):30125–30136.

61. Samsom M, Chan A, Iwabuchi Y, et al. 2015. In vitro friction testing of contact lenses and human ocular tissues: Effect of proteoglycan 4 (PRG4). Tribol. Int. 89:27–33.

62. Basalo IM, Mauck RL, Kelly TN, et al. 2004. Cartilage interstitial fluid load support in unconfined compression following enzymatic digestion. J. Biomech. Eng. 126(6):779–786 Available from: https://pubmed.ncbi.nlm.nih.gov/15796336.

63. Lyyra T, Arokoski JPA, Oksala N, et al. 1999. Experimental validation of arthroscopic cartilage stiffness measurement using enzymatically degraded cartilage samples. Phys. Med. Biol. 44(2):525–535 Available from: http://dx.doi.org/10.1088/0031-9155/44/2/017.

64. Rieppo J, Toyras J, Nieminen MT, et al. 2003. Structure-function relationships in enzymatically modified articular cartilage. Cells. Tissues. Organs 175(3):121–132.

65. Griffin DJ, Vicari J, Buckley MR, et al. 2014. Effects of enzymatic treatments on the depth-dependent viscoelastic shear properties of articular cartilage. J. Orthop. Res. 32(12):1652–1657.

66. Basalo IM, Raj D, Krishnan R, et al. 2005. Effects of enzymatic degradation on the frictional response of articular cartilage in stress relaxation. J. Biomech. 38(6):1343–1349.

67. Jay GD, Torres JR, Warman ML, et al. 2007. The role of lubricin in the mechanical behavior of synovial fluid. Proc. Natl. Acad. Sci. U. S. A. 104(15):6194–6199 [cited 2019

Jul 10] Available from: http://www.ncbi.nlm.nih.gov/pubmed/17404241.

68. Bloom AK, Samsom ML, Regmi SC, et al. 2019. Investigating the effect of proteoglycan 4 on hyaluronan solution properties using confocal fluorescence recovery after photobleaching. BMC Musculoskelet. Disord. 20(1):93 Available from: https://doi.org/10.1186/s12891-019-2469-4.

69. Critchley S, Sheehy EJ, Cunniffe G, et al. 2020. 3D printing of fibre-reinforced cartilaginous templates for the regeneration of osteochondral defects. Acta Biomater. 113:130–143 Available from: http://www.sciencedirect.com/science/article/pii/S1742706120303196.

70. Gonzalez JS, Alvarez VA. 2014. Mechanical properties of polyvinylalcohol/hydroxyapatite cryogel as potential artificial cartilage. J. Mech. Behav. Biomed. Mater. 34:47–56.

71. Maiolo AS, Amado MN, Gonzalez JS, Alvarez VA. 2012. Development and characterization of Poly (vinyl alcohol) based hydrogels for potential use as an articular cartilage replacement. Mater. Sci. Eng. C. Mater. Biol. Appl. 32(6):1490–1495.

72. Oungoulian SR, Durney KM, Jones BK, et al. 2015. Wear and damage of articular cartilage with friction against orthopedic implant materials. J. Biomech. 48(10):1957–1964.

73. Qian S, Zhang L, Ni Z feng, et al. 2017. Investigation of contact characteristics and frictional properties of natural articular cartilage at two different surface configurations. J. Mater. Sci. Mater. Med. 28(6):84 Available from: https://doi.org/10.1007/s10856-017-5895-6.

74. Chan SMT, Neu CP, Komvopoulos K, Reddi AH. 2011. The role of lubricant entrapment at biological interfaces: reduction of friction and adhesion in articular cartilage. J. Biomech. 44(11):2015–2020.

75. Caligaris M, Canal CE, Ahmad CS, et al. 2009. Investigation of the frictional response of osteoarthritic human tibiofemoral joints and the potential beneficial tribological effect of healthy synovial fluid. Osteoarthr. Cartil. 17(10):1327–1332.

76. Jones AR, Chen S, Chai DH, et al. 2009. Modulation of lubricin biosynthesis and tissue surface properties following cartilage mechanical injury. Arthritis Rheum 60 Available from: http://dx.doi.org/10.1002/art.24143.